AFRL-AFOSR-UK-TR-2016-0024

Anisoplanatic Imaging through Turbulence 140244

Szymon Gladysz
Fraunhofer Institute of Optronics

10/06/2016
Final Report

Air Force Research Laboratory
AF Office Of Scientific Research (AFOSR)/ IOE
Arlington, Virginia 22203
Air Force Materiel Command

REPORT DOCUMENTATION PAGE

Form Approved
OMB No. 0704-0188

1. REPORT DATE *(DD-MM-YYYY)*	2. REPORT TYPE	3. DATES COVERED *(From - To)*
07-10-2016	Final	15 Aug 2014 to 14 Aug 2016

4. TITLE AND SUBTITLE
Anisoplanatic Imaging through Turbulence

5a. CONTRACT NUMBER

5b. GRANT NUMBER
FA9550-14-1-0244

5c. PROGRAM ELEMENT NUMBER
61102F

6. AUTHOR(S)
Szymon Gladysz

5d. PROJECT NUMBER

5e. TASK NUMBER

5f. WORK UNIT NUMBER

7. PERFORMING ORGANIZATION NAME(S) AND ADDRESS(ES)
Fraunhofer Institute of Optronics
System Technologies and Image Exploitation IOSB
Gutleuthausstraße 1, 76275 Ettlingen, Germany Phone +49 7243
992 120 ES

8. PERFORMING ORGANIZATION REPORT NUMBER

9. SPONSORING/MONITORING AGENCY NAME(S) AND ADDRESS(ES)
EOARD
Unit 4515
APO AE 09421-4515

10. SPONSOR/MONITOR'S ACRONYM(S)
AFRL/AFOSR IOE

11. SPONSOR/MONITOR'S REPORT NUMBER(S)
AFRL-AFOSR-UK-TR-2016-0024

12. DISTRIBUTION/AVAILABILITY STATEMENT
A DISTRIBUTION UNLIMITED: PB Public Release

13. SUPPLEMENTARY NOTES

14. ABSTRACT
The activities in Year 2 have followed two main research directions:
- The development of a new point-spread function (PSF) reconstruction approach which aims at extracting, from multi-frame observations, a number of PSFs at several locations within an image of an arbitrary object (without point sources).
- The development of a marginal blind deconvolution estimator, combined with constraints on the observed object such as positivity, for identification of long-exposure adaptive optics PSFs. This approach can also be extended to the anisoplanatic case by its application in different locations of the field of view as a first building block of a global shift-variant image restoration approach.
The approaches are complementary to each other. From the first approach it is possible to extract a model for the object's power spectral density that can be used to complete the parameters to be used in the second approach.

15. SUBJECT TERMS
EOARD, Adaptive Optics, EO imaging, anisoplanatic, space surveillance, optronics, multi-conjugate AO

16. SECURITY CLASSIFICATION OF:			17. LIMITATION OF ABSTRACT	18. NUMBER OF PAGES	19a. NAME OF RESPONSIBLE PERSON
a. REPORT	b. ABSTRACT	c. THIS PAGE			MILLER, KENT
Unclassified	Unclassified	Unclassified	SAR	19	19b. TELEPHONE NUMBER *(Include area code)* 011-44-1895-616022

Dr. Szymon Gładysz 18 July 2016

Fraunhofer Institute of Optronics,
System Technologies and Image Exploitation IOSB
Gutleuthausstraße 1, 76275 Ettlingen, Germany
Phone +49 7243 992 120
szymon.gladysz@iosb.fraunhofer.de

Grant number FA9550-14-1-0244

"Anisoplanatic Imaging through Turbulence"

Interim report

Period of performance: 15 August 2015 - 14 August 2016

Table of Contents

List of Figures

1. Summary

In this document we report on activities related to the project "Anisoplanatic Imaging through Turbulence", grant number FA9550-14-1-0244. The activities in Year 2 have followed two main research directions:

- The development of a new point-spread function (PSF) reconstruction approach which aims at extracting, from multi-frame observations, a number of PSFs at several locations within an image of an arbitrary object (without point sources) (Section 3.1).
- The development of a marginal blind deconvolution estimator, combined with constraints on the observed object such as positivity, for identification of long-exposure adaptive optics PSFs. This approach can also be extended to the anisoplanatic case by its application in different locations of the field of view as a first building block of a global shift-variant image restoration approach (Section 3.2).

Both approaches are complementary to each other, e.g., from the first approach it is possible to extract a model for the object's power spectral density that can be used to complete the parameters to be used in the second approach.

2. Introduction

The performance of optical systems is degraded by atmospheric turbulence when observing vertically (e.g. astronomy) or horizontally (e.g. surveillance, military reconnaissance). This degradation can be alleviated in software (real-time de-blurring or post-processing) or hardware (adaptive optics – AO). Tremendous progress has been achieved in this area: in astronomy almost every major observatory is now equipped with first-generation AO systems and some second-generation systems are currently coming online. High-resolution imaging of satellites is now a routine task at the Air Force Maui Optical and Supercomputing (AMOS) observatory thanks to a combination of AO and post-processing. The technology and associated image processing techniques have been successfully transferred to commercial markets, especially in the field of ophthalmic imaging.

One problem still remains: Adaptive optics systems are generally only capable of correcting very small fields of view. In single-conjugated AO systems, i.e., ones that measure and correct atmospheric distortions in one direction, with a single deformable mirror, the usable field-of-view is determined by the so-called isoplanatic angle (Figure 1). This angle describes the field-of-view in which turbulence-induced aberrations could be considered constant and therefore correctable with a single device. In other words, given a certain correction direction, isoplanatic angle gives the maximum angular separation from this direction at which reasonably good correction can be expected. In conventional AO systems, the correctable field-of-view has a size of the order of isoplanatic angle.

In theory, the problem of wide-field imaging can be solved by multi-conjugate AO. Such systems, already deployed successfully at a handful of astronomical observatories, correct aberrations resulting from propagations over distinct paths using a number of wavefront sensors and corresponding deformable mirrors. These systems are complex, bulky, one-off instruments. In astronomical imaging, two-three wavefront sensors and deformable mirrors already increase the field of view to enable new science.

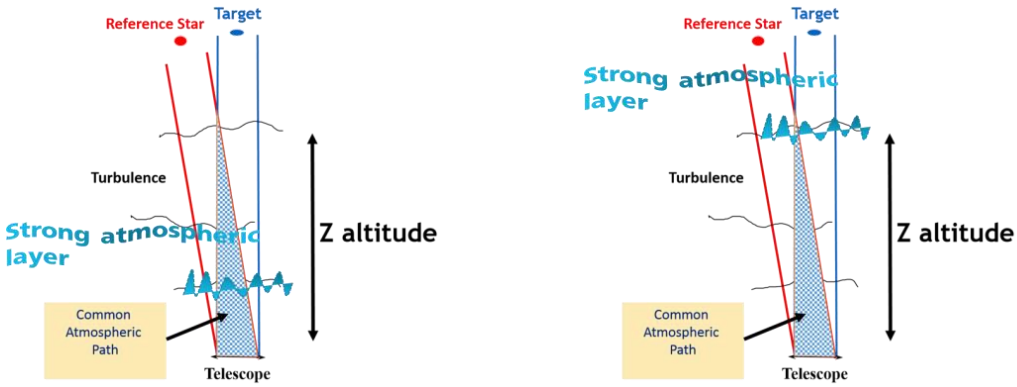

Fig. 1. Illustration of the problem of anisoplanatism in imaging through turbulence with adaptive optics, vertical-path scenario. Left: when strong atmospheric layer is located close to the telescope pupil then there exists a large overlap in significant wavefront aberrations between light coming from the object of interest and the guide star (reference for AO). Right: when the layer of significant turbulence is located further up then the overlap between the wavefronts coming from the two directions is reduced and subsequently the correction applied to the deformable mirror is valid only for the reference star and not for the target.

This solution is not applicable for at least two areas of interest: For ground-level surveillance, where the field of view could extend over hundreds of isoplanatic patches because of the strength of turbulence along horizontal paths near the ground, multi-conjugate AO would have to consist of hundreds of wavefront sensors and corresponding deformable mirrors. This poses an enormous technical problem and the idea of multi-conjugate AO in this context is currently not being followed. Also, in air-to-ground, "looking-down" scenario, the ratio of sensor aperture to the coherence length of the atmosphere is around unity (as opposed to tens or hundreds in imaging from the ground) but isoplanatic angles are usually very small because optical aberrations are located far away from the imaging pupil.

The hardware solution to the problem of anisoplanatism, i.e. multi-conjugate AO, is very expensive. Therefore, in this project we follow two software approaches.

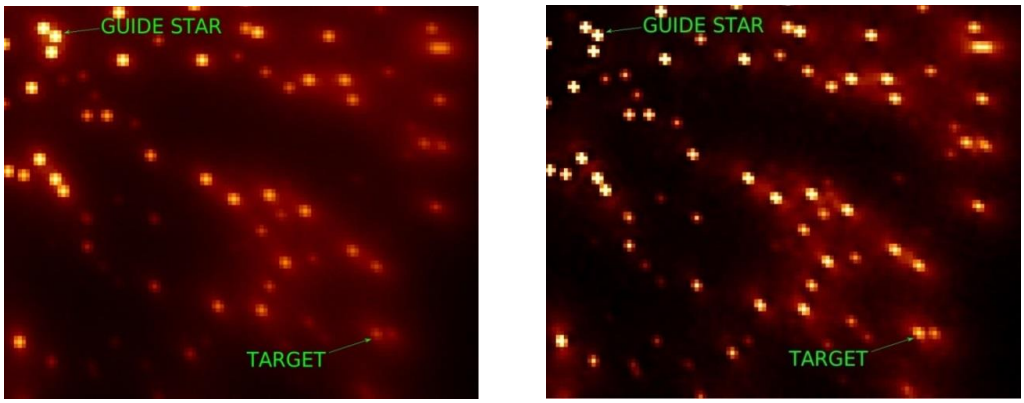

Fig. 2. Simulated data showing a stellar field imaged with single-conjugate AO (for more details on the simulation see [1]). Left: original data, false color and stretched scale. Right: result of image reconstruction with a single PSF corresponding to the guide star, ignoring anisoplanatism. It can be seen how image quality degrades when moving away from the guide star.

Data from single-conjugate AO systems are difficult to post-process (deconvolve) because of the spatially-variant blur (Figure 2). This means that each point in an image is blurred by a slightly different point-

spread function (PSF). On the other hand, almost all deconvolution algorithms rely on PSF being constant in the field of view. This is the shift-*invariant* paradigm which does not lead to optimal results (cf. right panel of Figure 2). In the following sections we describe two solutions which we followed to tackle this problem.

3. Methods, Assumptions, and Procedures

3.1 PSF reconstruction directly from target data

In the first year of the project work was performed on reformulation of imaging problem from traditional shift-invariant into the shift-*variant* case, development of simulations of anisoplanatic imagery and anisoplanatic image reconstruction algorithms. Gains have been made on all three fronts but the underlying assumption was that the algorithms have access to knowledge about the form of the PSF at every point in an image. In the second year, efforts were devoted to finding an approach that could reveal these PSFs even for objects without features such as edges or bright points. As mentioned in the grant proposal, building on our previous work on object-cancelling transformations [2] we hoped to find new transformations which would allow to reduce the problem to two equations with two unknowns, giving directly the PSF. Ultimately, this proved possible and good results have been obtained (see Section 4.1).

The imaging equation for a true object $\mathbf{o}(\vec{x})$ convolved with a PSF $\mathbf{h}(\vec{x})$, giving the recorded image $\mathbf{i}(\vec{x})$ is:

$$\mathbf{i}(\vec{x}) = \mathbf{o}(\vec{x}) \otimes \mathbf{h}(\vec{x}) \tag{1}$$

where $\otimes$ denotes the convolution operator and the symbol $\vec{x}$ corresponds to two-dimensional focal-plane coordinate. Equation (1), transformed into Fourier domain, squared and averaged over *M* images, becomes:

$$\left\langle \left|\mathbf{I}(\vec{u})\right|^2 \right\rangle_M = \left|\mathbf{O}(\vec{u})\right|^2 \left\langle \left|\mathbf{H}(\vec{u})\right|^2 \right\rangle_M \tag{2}$$

If we gain access to the AO speckle transfer function $\left\langle \left|\mathbf{H}(\vec{u})\right|^2 \right\rangle_M$ then the AO modulation transfer function (MTF) $\left|\left\langle \mathbf{H}(\vec{u}) \right\rangle\right|$ can be directly obtained (see Equation (7)). A PSF is then derived by Fourier transforming the MTF. Although the phase of the optical transfer function (OTF) $\left\langle \mathbf{H}(\vec{u}) \right\rangle$ is lost in the process, we show that the approach still yields a useful PSF.

In order to break the symmetry of Equation (2) we cancel out the object by transforming it into equations involving moments of $\left|\mathbf{H}(\vec{u})\right|^2$. One such transformation, termed "Fourier contrast", was already discovered by us before [2]. It is given by standard deviation of the power spectrum computed for each frequency separately, divided by the mean value of the power spectrum at this frequency:

$$C\left(\left|\mathbf{I}(\vec{u})\right|^2\right) = \frac{\left|\mathbf{O}(\vec{u})\right|^2}{\left|\mathbf{O}(\vec{u})\right|^2} \frac{\sqrt{\left\langle \left|\mathbf{H}(\vec{u})\right|^4 \right\rangle - \left\langle \left|\mathbf{H}(\vec{u})\right|^2 \right\rangle^2}}{\left\langle \left|\mathbf{H}(\vec{u})\right|^2 \right\rangle} \tag{3}$$

If the object is static during the observations then its power spectrum cancels out and we are left only with the part involving random aberrations. Note that all static terms disappear from the result, i.e. also telescope OTF will be removed. Therefore in order to obtain realistic PSF one has to multiply the result of the method again by the telescope OTF, preferably one which includes also static errors of the optics. Some practical issues related to this process are discussed in Section 4.1.

Naturally, from the statistical moments of the AO speckle transfer function it is not possible to derive its mean value. The second transformation that cancels out the static object is Fourier skewness [3]:

$$S\left(\left|\mathbf{I}(\vec{u})\right|^2\right) = \frac{\left|\mathbf{O}(\vec{u})\right|^6}{\left|\mathbf{O}(\vec{u})\right|^6} \frac{\left\langle\left|\mathbf{H}\right|^6\right\rangle - 3\left\langle\left|\mathbf{H}\right|^4\right\rangle\left\langle\left|\mathbf{H}\right|^2\right\rangle + 2\left\langle\left|\mathbf{H}\right|^2\right\rangle^3}{\left(\left\langle\left|\mathbf{H}\right|^4\right\rangle - \left\langle\left|\mathbf{H}\right|^2\right\rangle^2\right)^{\frac{3}{2}}} \tag{4}$$

The transformation amounts to computing the third standardized moment of the image power spectra, separately for each frequency. If the object does not change during the observations then it will cancel out from Equation (4).

Equations (3) and (4) involve many higher-order moments of $\left|\mathbf{H}(\vec{u})\right|^2$. In order to arrive at a tractable formulation of the problem we must express these moments using as few parameters as possible. Although in general, the AO OTF is modeled with many variables corresponding to the parameters of the turbulence and the AO system [4-6], here we use a much simpler model. We start with the realization that the OTF is a speckle [2]:

$$\mathbf{H}(\vec{u}) = \frac{1}{N}\sum_{i=1}^{N} e^{j\left(\theta(\xi_i,\eta_i) - \theta(\xi_i + \bar{\lambda} z u_X, \eta_i + \bar{\lambda} z u_Y)\right)} \tag{5}$$

where ξ,η are the pupil-plane coordinates, $\bar{\lambda}$ is the average wavelength of the observations, z is the distance from the exit pupil to the image plane, N is the number of OTF cells in the area of overlap [2] and θ's are the phases – identically distributed random variables.

Note that because phases are random the OTF also has to be random, even for long exposures. Given this realization, one can write moments of $\left|\mathbf{H}(\vec{u})\right|^2$ using only the following parameters: N, which is of little practical interest, and various powers of the OTF [7]. These expressions are very long but fortunately approximations have been derived for the case of large N [8]. For contrast and skewness one obtains, respectively:

$$\begin{aligned} C &\approx \sqrt{\frac{2}{N}} \frac{1 - \left\langle\left|\mathbf{H}\right|^2\right\rangle}{\sqrt{\left\langle\left|\mathbf{H}\right|^2\right\rangle}}, \quad N >> 1 \\ S &\approx \frac{1}{\sqrt{2N}} \frac{3 - 6\left\langle\left|\mathbf{H}\right|^2\right\rangle - \left\langle\left|\mathbf{H}\right|^2\right\rangle^2}{\sqrt{\left\langle\left|\mathbf{H}\right|^2\right\rangle}}, \quad N >> 1 \end{aligned} \tag{6}$$

Looking at Equation (6) we see that we obtained two equations with two unknowns: the modulation transfer function $|\mathbf{H}|$ and the number of OTF cells *N*. One can now proceed to calculate modulation transfer function for any object being imaged. Beforehand, one last simplification in Equation (6) is used:

$$\left\langle |\mathbf{H}(\vec{u})|^2 \right\rangle = \frac{1}{N}\left[1+(N-1)\exp\left(-D_\theta(\bar{\lambda}\, zu_X, \bar{\lambda}\, zu_Y)\right)\right] \approx \exp\left(-D_\theta(\bar{\lambda}\, zu_X, \bar{\lambda}\, zu_Y)\right) \approx \left|\langle \mathbf{H}(\vec{u})\rangle\right|^2, \quad N >> 1 \quad (7)$$

where $D_\theta(.)$ is the structure function of the AO residual phase. This approximation is only valid for AO-compensated imaging.

To summarize, the new approach to AO PSF reconstruction involves the recording of several exposures of the same object, computing contrast and skewness of the power spectra of the data, obtaining the AO MTF from Equations (6) and (7) and Fourier-transforming it to derive the average PSF of the observations. As mentioned before, unfortunately the OTF phase information is lost in the process.

3.2 Marginal blind deconvolution for satellite identification

Blind deconvolution, both in the astronomical context and for satellite identification, is usually performed in a joint fashion, i.e., object and PSF are estimated together alternating the minimization of a certain cost function between one and the other. However, it is now well known that this often produces a solution that is degenerate and, when it works, it is thanks to some constraints and prior information about the PSF and/or the object, such as positivity, which help algorithms converge to a reasonable solution.

In a nutshell, joint blind deconvolution consists in maximizing the joint probability p(**i,o,h**), where **i** is the image or data, and **o** and **h** are the unknown object and PSF to be recovered. If the PSF is considered a linear combination of a set of modes $\{\mathbf{h}_j\}_{j=1\ldots J}$, i.e., $\mathbf{h} = \sum_{j=1}^{J} \alpha_j \mathbf{h}_j$, where the set of **{α}** are the coefficients that parameterize the PSF, then the joint probability to be maximized would be p(**i,o,α**). This change of parameter (from **h** to **α**) allows us to reduce the number of unknowns from the number of pixels on the PSF support to a few coefficients. If the modes are also PSFs then the set of coefficients is normalized to 1 ($\sum_{j=1}^{J} \alpha_j = 1$) and each of them is positive ($\alpha_j > 0$).

In the case where the noise is assumed stationary white Gaussian, and a Gaussian prior distribution with mean value $\boldsymbol{o_m}$ is also assumed for the object, then the joint criterion to be minimized $J_{j(\text{oint})MAP}$, which is the opposite of the logarithm of the joint probability p(**i,o,α**), adopts the following expression [9]:

$$J_{jMAP}(\boldsymbol{o},\boldsymbol{\alpha}) = \frac{1}{2}\sum_{\vec{u}} \frac{|\boldsymbol{I}(\vec{u}) - \boldsymbol{H}(\vec{u})\boldsymbol{O}(\vec{u})|^2}{S_n} + \frac{1}{2}\sum_{\vec{u}} \frac{|\boldsymbol{O}(\vec{u}) - \boldsymbol{O_m}(\vec{u})|^2}{\boldsymbol{S_o}(\vec{u})} + C \quad (8)$$

where $\vec{u}$ is a two-dimensional spatial frequency coordinate, S_n and $\boldsymbol{S_o}$ are, respectively, the noise and object power spectral densities (PSD), and capital letters denote the 2-D Fourier Transform. In Equation (8) if we replace the object by the Wiener solution for a given set of **{α}** we obtain a new expression that does not depend explicitly on the object.

$$J_{jMAP}(\boldsymbol{o_W}(\boldsymbol{\alpha}),\boldsymbol{\alpha}) = \frac{1}{2}\sum_{\vec{u}} \frac{1}{\boldsymbol{S_o}(\vec{u})} \frac{|\boldsymbol{I}(\vec{u}) - \boldsymbol{H}(\vec{u})\boldsymbol{O_m}(\vec{u})|^2}{|\boldsymbol{H}(\vec{u})|^2 + \frac{S_n}{\boldsymbol{S_o}(\vec{u})}} + C \quad (9)$$

It is important to notice that $J_{jMAP}(\boldsymbol{o},\boldsymbol{\alpha})$ and $J_{jMAP}(\boldsymbol{o_W}(\boldsymbol{\alpha}),\boldsymbol{\alpha})$ are equivalent, i.e., the use of the Wiener solution does not change the shape of the criterion but only the speed at which it is minimized. From Equation (9) it is easy to understand why the joint solution is degenerate: if the mean object $\boldsymbol{o_m}$ is constant, and since the PSF as well as the set of coefficients $\{\boldsymbol{\alpha}\}$ are normalized to 1, the numerator does not depend on such set of coefficients $\{\boldsymbol{\alpha}\}$. Minimizing J_{jMAP} is equivalent to maximizing the denominator, i.e., choosing the PSF with the highest$|\boldsymbol{H}(\vec{u})|$, which is the sharpest PSF. Therefore the solution of the optimization of this joint criterion is always the sharpest PSF, whatever the true PSF may be!

A possible solution to this problem is the use of the marginal estimator. Its goal is to estimate the set of most likely coefficients $\{\boldsymbol{\alpha}\}$ on average for all possible objects by integrating the object **o** out of the problem, i.e., we integrate the joint probability on all possible objects. In other words, the joint estimation consists in maximizing p(**i,o,α**), whereas the marginal estimation consists in maximizing $\int_{\mathbf{o}}$p(**i,o,α**), i.e., maximizing the joint probability over all possible objects, which is the marginal probability p(**i,α**),. Marginalization reduces the number of unknowns providing an expression that only depends on the set of PSF coefficients $\{\boldsymbol{\alpha}\}$. Once these coefficients are estimated they are used to restore the object, for instance by Wiener filtering of the image. If we again assume a Gaussian distribution for noise, and no prior information for the set of $\{\boldsymbol{\alpha}\}$, then the expression of the marginal criterion is [9]:

$$J_{ML}(\boldsymbol{\alpha}) = \frac{1}{2}\sum_{\vec{u}} \frac{1}{\boldsymbol{S_o}(\nu)} \frac{|\boldsymbol{I}(\vec{u}) - \boldsymbol{H}(\vec{u})\boldsymbol{O_m}(\vec{u})|^2}{|\boldsymbol{H}(\vec{u})|^2 + \frac{S_n}{\boldsymbol{S_o}(\vec{u})}} + \frac{1}{2}\sum_{\vec{u}} \ln\left(|\boldsymbol{H}(\vec{u})|^2 + \frac{S_n}{\boldsymbol{S_o}(\vec{u})}\right) + C \tag{10}$$

Equation (10) is very similar to Equation (9) however the presence of $|\boldsymbol{H}(\vec{u})|^2$ in the additional term provides the marginal criterion with better properties with respect to the joint one, as can be seen in Figure 3.

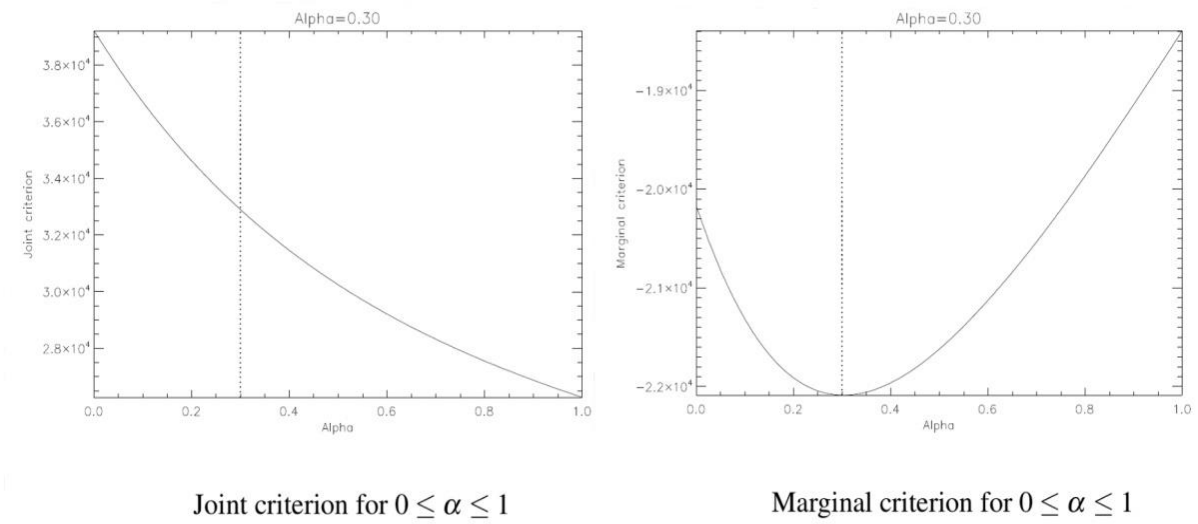

Fig. 3. Plot for the joint (left) and the marginal (right) estimator when the PSF is a linear combination of two modes related with one single coefficient of value α=0.3, i.e., $\boldsymbol{h} = \alpha \cdot \boldsymbol{h_{foc}} + (1-\alpha) \cdot \boldsymbol{h_{defoc}}$. The reader can notice that the marginal criterion has its minimum at the correct value of α, whereas the joint criterion has its minimum for that α that pushes the PSF to be the focused one, i.e., the sharpest one.

From Equations (8) and (10) is easy to realize that the marginal and the joint criteria are related when the Wiener solution is used for the latter:

$$J_{ML}(\boldsymbol{\alpha}) = J_{jMAP}(\boldsymbol{o_W}(\boldsymbol{\alpha}), \boldsymbol{\alpha}) + \frac{1}{2}\sum_{\vec{u}} \ln\left(|\boldsymbol{H}(\vec{u})|^2 + \frac{S_n}{\boldsymbol{S_o}(\vec{u})}\right) + C \tag{11}$$

If we do not impose the Wiener solution in the joint criterion, we can create a new criterion derived from the marginal one, but with the explicit presence of the object:

$$J_{ML}(\boldsymbol{o}, \boldsymbol{\alpha}) = J_{jMAP}(\boldsymbol{o}, \boldsymbol{\alpha}) + \frac{1}{2}\sum_{\vec{u}} \ln\left(|\boldsymbol{H}(\vec{u})|^2 + \frac{S_n}{\boldsymbol{S_o}(\vec{u})}\right) + C \tag{12}$$

This new criterion can be minimized alternating between the object and the PSF coefficients, and the explicit presence of the object allows us to impose strong constraints over it, such as positivity, during the optimization. In practice, the positivity constraint behaves as an object support constraint and it is especially useful in the astronomical context and for satellite identification, where objects to be recovered usually lie over a black background. The drawback of using the non-analytical solution in $J_{jMAP}(\boldsymbol{o}, \boldsymbol{\alpha})$ instead of the Wiener one is a decrease in the speed of convergence, since the minimization is again performed alternately between the object and the PSF.

Then, the final expression for the new marginal criterion with positivity on the object is:

$$J_{ML}(\boldsymbol{o}, \boldsymbol{\alpha})|_{\text{s.t. } \boldsymbol{o}>0} = \frac{1}{2}\sum_{\vec{u}} \frac{|\boldsymbol{I}(\vec{u}) - \boldsymbol{H}(\vec{u})\boldsymbol{O}(\vec{u})|^2}{S_n} + \frac{1}{2}\sum_{\vec{u}} \frac{|\boldsymbol{O}(\vec{u}) - \boldsymbol{O_m}(\vec{u})|^2}{\boldsymbol{S_o}(\vec{u})} + \frac{1}{2}\sum_{\vec{u}} \ln\left(|\boldsymbol{H}(\vec{u})|^2 + \frac{S_n}{\boldsymbol{S_o}(\vec{u})}\right) + C \tag{13}$$

Where the first term in Equation (13) is the data fidelity term when stationary white Gaussian noise is considered, the second term is a Gaussian prior distribution for the object, with an explicit presence of it, and the third term is due to the marginalization.

Finally, the marginal criterion, either with or without positivity, needs the object and noise PSDs $\boldsymbol{S_o}(\vec{u})$ and S_n. Fortunately, both can be estimated together with the PSF coefficients in an automatic manner during the minimization. In order to reduce the number of new parameters to estimate, a simple model for the object PSD was chosen, e.g., $\boldsymbol{S_o} = \frac{k}{1+\left(\frac{\vec{u}}{\vec{u}_0}\right)^p}$. This model has been previously used with success in both the astronomical context and in ground-based imaging of satellites [10], and it only adds 3 new parameters $\{k, \vec{u}_0, p\}$ together with the noise PSD, which is constant since we are assuming white noise.

4. Results and Discussion

4.1 PSF reconstruction applied to simulated and real data

In order to test the PSF reconstruction method described in Section 3.1 we first performed tests on images where the ground-truth average PSF was known with a high degree of accuracy: a large set of AO PSFs with high signal-to-noise ratio. A sequence of 4000 short exposure images (t_{exp} = 22 ms) of a single bright star taken with the 3-m Shane Telescope at the Lick Observatory was used. Images were taken in K-band (2.2 μm) with AO (7×7 actuators on the deformable mirror) switched on. The resulting Strehl ratio was 53%. Power spectra were computed for each image and subsequently contrast and skewness values of each frequency component were computed, i.e. statistical quantities were averaged over time.

As mentioned in Section 3.1, the proposed operations on the data remove all static components of the images, including the ones that must be modelled accurately to capture image degradation. While it is straightforward to re-introduce the OTF of the telescope with an arbitrarily shaped pupil back into the result of the method, it is not that straightforward to recover the information about the static aberrations that gets lost in the process. This is an issue common to all PSF reconstruction approaches [6]. Here we use a PSF obtained from fiber measurements with the telescope dome closed, i.e. a PSF only affected by static optical aberrations. This PSF is convolved with the AO-residual PSF, or alternatively their respective OTFs are multiplied.

The azimuthally-averaged results of applying the described method are shown in the left panel of Figure 4. In the right panel we show the corresponding images of PSFs. These first results are very encouraging. The true and estimated MTFs overlap and structure of the PSF is well represented (note the AO correction zone, roughly 14 pixels in size, in panel **c**). The results are more than satisfactory given that the fiber PSF was taken around two years after the first observations.

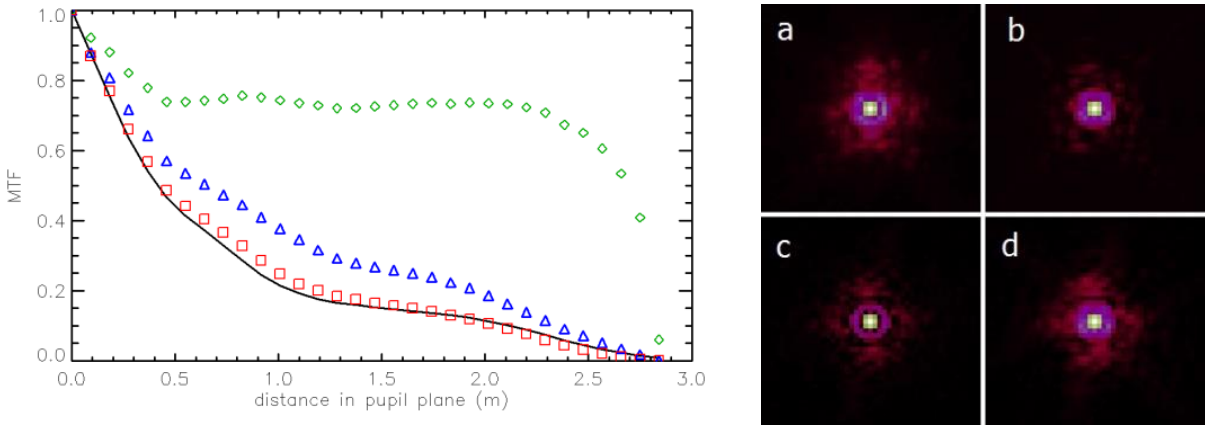

Fig. 4. Illustration of the method's performance. Left: Black line: ground truth, i.e. the MTF corresponding to the observations. Green diamonds: estimated MTF of the turbulence AO-residuals only. Blue triangles: estimated AO MTF (green diamonds) multiplied by the perfect, diffraction-limited MTF. Red squares: AO MTF multiplied by the MTF containing the telescope and static error terms (taken from a fiber PSF). Right: (a) ground truth – in this case real PSF, (b) fiber PSF (no turbulence, only static errors), (c) result of PSF reconstruction after inclusion of the perfect, diffraction-limited MTF, (d) result of PSF reconstruction after inclusion of the information from the fiber PSF.

Given these very encouraging results, we proceeded to tackle a much more challenging but also much more realistic scenario of an extended object which changes throughout the observations. Data was kindly provided by AFRL staff involved in this project. The set comprises 100 short exposures (t_{exp} = 15 ms) of a defunct US remote-sensing satellite Seasat taken with the 3.5-m telescope at the Starfire Optical Range, New Mexico. Observations were carried out in the laser-guide star AO mode, with 24×24 actuators on the deformable mirror. Wavelength of the observations was 0.8 μm. It is estimated that the Strehl ratio of the observations is in the range 10-30 %. Figure 5 shows some frames from the sequence.

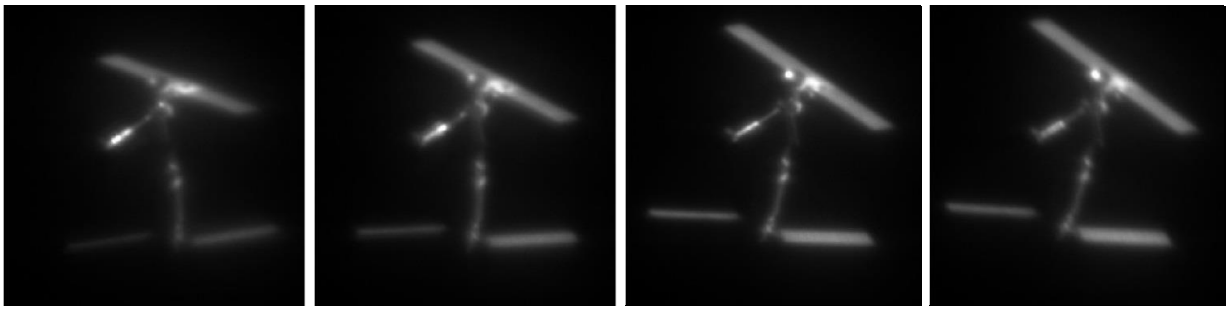

Fig. 5. Example frames from the Seasat sequence. Note the appearance and disappearance of glints, change in aspect and local illumination of the satellite and the rotation with respect to the observer.

There are two challenging aspects associated with the application of the described PSF reconstruction method on this data. Firstly, the object is rapidly changing: the satellite is rotating, tumbling, changing aspect, glinting, etc. Secondly, in contrast to celestial objects, the satellite's overhead movement is very fast and the level of AO correction changes throughout the sequence. In order to obtain meaningful PSFs, the sequence was therefore divided into subsequences. This was a trade-off study: for shorter subsequences the object is more constant but PSF estimation is less accurate because of small samples. Longer subsequences have better signal-to-noise ratio on the estimators but the variability of the object leaks through Equations (3) and (4). After a trade-off study a subsequence length of 25 frames was found optimal for these observations. Figure 6 shows input image centered in the middle of one such subsequence, the reconstructed PSF, as well as the results of various deconvolution algorithms which were supplied with this PSF. The algorithms did not update the PSF; they simply used it as it was (non-blind mode). The improvement in image quality with regard to the original data shows that the reconstructed PSF is useful. Naturally, a more advanced deconvolution algorithm could update this first-guess PSF ("myopic" mode) and offset the errors which arise in the PSF reconstruction part due to e.g. changes in the object or estimation noise.

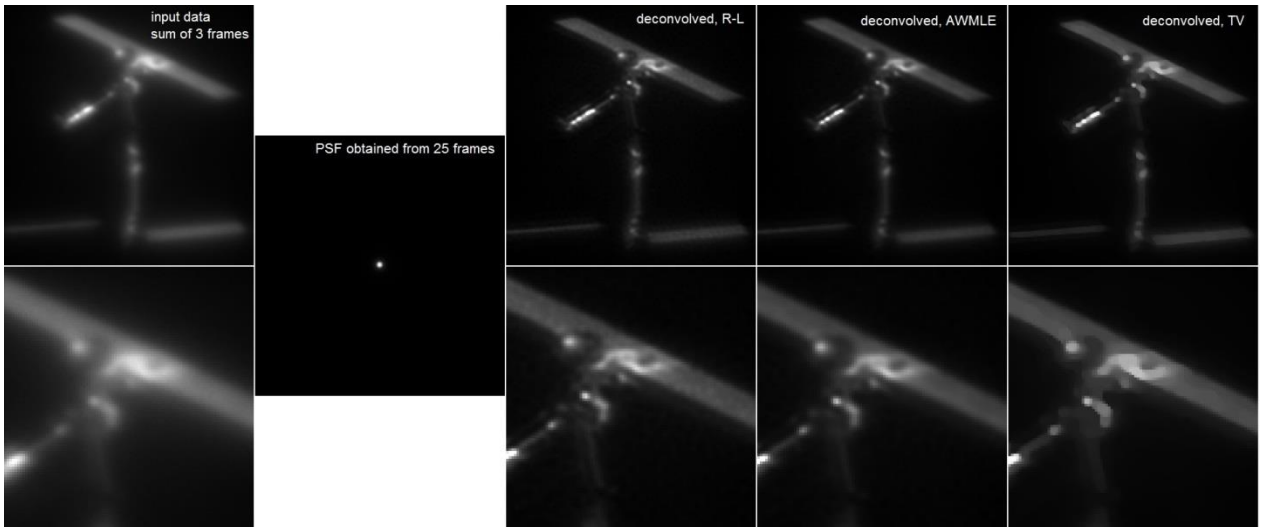

Fig. 6. Left: input data whereby three short-exposure frames were summed to increase the signal-to-noise ratio. Second from left: reconstructed PSF. Center: input data deconvolved with the reconstructed PSF and the Richardson-Lucy algorithm (R-L). Second from right: deconvolution result with the AWMLE algorithm [11]. Far right: deconvolution with the total variation regularization.

How can this new method be used to tackle the problem of anisoplanatic deconvolution? In the third year of the project it will be combined with the image decomposition approach developed in the first year: we studied ways of optimally describing an anisoplanatic image in terms of the principal components of the spatially-varying PSF. Now we have a way to find the local PSFs. Rewriting Equation (1) for the anisoplanatic case we have:

$$\mathbf{i}(\vec{x}) = \mathbf{o}(\vec{v}) \otimes \mathbf{h}(\vec{v}, \vec{x}) + \mathbf{n}(\vec{x}) \tag{14}$$

This time we have deliberately included noise $\mathbf{n}(\vec{x})$ in the equation. The symbols $\vec{x}$ and $\vec{v}$ are 2-D vectors denoting image-, and object-space coordinates, respectively. Note that the PSF is assumed to change with $\vec{v}$ and $\vec{x}$. We assume that the set of reconstructed PSFs can be decomposed into *J* principal components $\mathbf{h}_j$ via singular value decomposition:

$$\mathbf{h}(\vec{v}, \vec{x}) \approx \sum_{j=1}^{J} \alpha_j(\vec{v}) \cdot \mathbf{h}_j(\vec{x}) \tag{15}$$

Then Equation (14) becomes:

$$\mathbf{i}(\vec{x}) \approx \sum_{j=1}^{J} \left[\left(\boldsymbol{\alpha}_j \cdot \mathbf{o} \right) \otimes \mathbf{h}_j \right](\vec{x}) + \mathbf{n}(\vec{x}) \tag{16}$$

The deconvolution process would then involve inverting Equation (16), possibly under some regularization, in order to obtain the object $\mathbf{o}(\vec{x})$. Because in practice the PSFs are most probably only going to be recoverable at a limited number of locations, the coefficients $\boldsymbol{\alpha}_j$ are going to be sparse. Some interpolation would have to be employed in order to obtain a map of $\boldsymbol{\alpha}_j$ covering the whole object. A regularized inversion of Equation (16) would then allow to offset the three sources of error: PSF reconstruction error, coefficient spatial interpolation error and the influence of noise.

4.2 Marginal blind deconvolution applied to simulated data

For testing of the marginal criterion on images of satellites, a set of 6 AO long-exposure PSFs were simulated analytically using the PAOLA package [12]. The simulations were carried out for the 3.5-m Starfire Optical Range telescope located at a site of rather bad seeing in New Mexico. A common value of $1.2''$ for seeing was adopted (the seeing angle is defined as the full-width-at-half-maximum of the long-exposure PSF taken through turbulence at 500 nm wavelength through an arbitrarily large telescope). With Nyquist-sampled PSFs (two pixels per λ/D) a 256×256 pixel field of view (FOV) covers $7.5''$. The magnitude of the guide star (GS) was set to 10 in the visible, the overall transmission from GS to detector was set to 15%. The zenith angle was set to 30°. The wavelength of the observations was set to 1 μm. The AO system has many parameters but most of them are outside the scope and interest of this report. The most important parameter is the density of actuators on the deformable mirror and simulations followed the current design of the SOR AO system with 24×24 actuators. The other parameters were either taken from SOR AO design documents [13] or optimized to obtain the highest Strehl ratio on axis. Moreover, simulated PSFs were obtained with two real turbulence profiles which had been obtained in the course of site testing in the context of the European Extremely Large Telescope project [14]. One profile has strong

ground-level turbulence and produces little anisoplanatism while the contrary is true for the second profile.

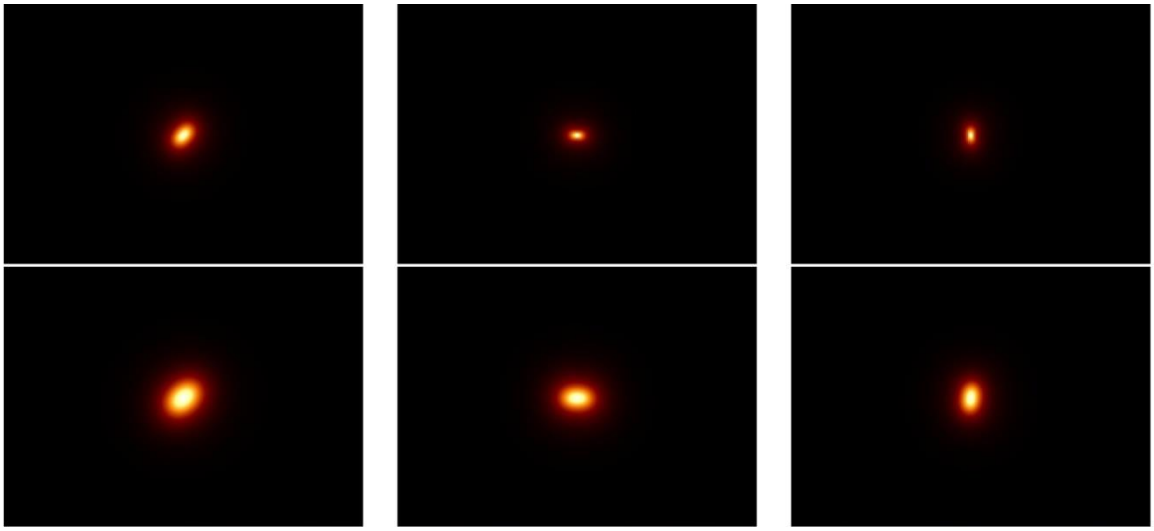

Fig. 7. Simulated set of PSFs in anisoplanatic conditions for two different atmospheric profiles (rows) and three different positions (columns)

In the simulations, firstly a GS image was generated and put in the top right corner of the FOV. Then, a loop over positions generated a PSF for the desired locations in the FOV according to its field angle and orientation with respect to the GS. These PSFs were then stored for subsequent convolution/deconvolution and are shown in Figure 7. As test object we used the schematic image of the Operationally Responsive Space-1 satellite (ORS) depicted in Figure 9. A test image was produced by convolving the test object with one of the six PSFs. Subsequently, shot noise and read out noise ($1e^-$ RMS) were added to produce the final images. Two different levels of noise were considered assuming different mean fluxes for the object, equal to 10^3 and 10^4 photons per pixel.

Finally, the marginal criterion, with and without positivity on the object, was tested over these images to obtain the coefficients that synthesized the PSF, to assess how well we can recover the true PSF out of the set of six simulated ones. The final goal is to recover a good PSF that can be used with whatever non-blind deconvolution algorithm we wish to use. Here, we have used the natural output of each approach, i.e., for the marginal criterion with positivity an explicit object is obtained at each iteration, hence, in Figure 9 we show the object at the last iteration. For the marginal criterion with no positivity the object is computed implicitly during the minimization process by means of the Wiener solution, i.e., there is no object at the last iteration. Therefore, in order to produce the final result we used the recovered PSF and object PSD together with a Wiener filter.

Table 1 and Figures 8 and 9 show the results of the marginal estimator when the image was simulated for the PSF number 3 (top row, third column) in Figure 7. This is a representative result for the rest of the tested PSFs. Table 1 shows that the marginal criterion is a powerful tool to estimate the correct PSF for long exposure AO observations, from a single image. The coefficient corresponding to the PSF which created the image was correctly identified by the estimator, with more robustness when the positivity on the object was applied. Figure 8 shows the recovered PSFs and Figure 9 the final reconstructed object with the corresponding PSF, either with or without positivity.

Table 1. Results of the marginal estimator applied to test data created with the PSF in the top row and third column in Figure 7. The input data is shown in Figure 9

		α_1	α_2	α_3	α_4	α_5	α_6
	True values	0	0	1	0	0	0
High SNR 10^4 ph/pixel	*Marginal + Positivity*	0	0	1	0	0	0
High SNR 10^4 ph/pixel	*Marginal*	0	0.0920	0.9079	0	0	0
Low SNR 10^3 ph/pixel	*Marginal + Positivity*	0	0	1	0	0	0
Low SNR 10^3 ph/pixel	*Marginal*	0	0.0211	0.7072	0	0.2717	0

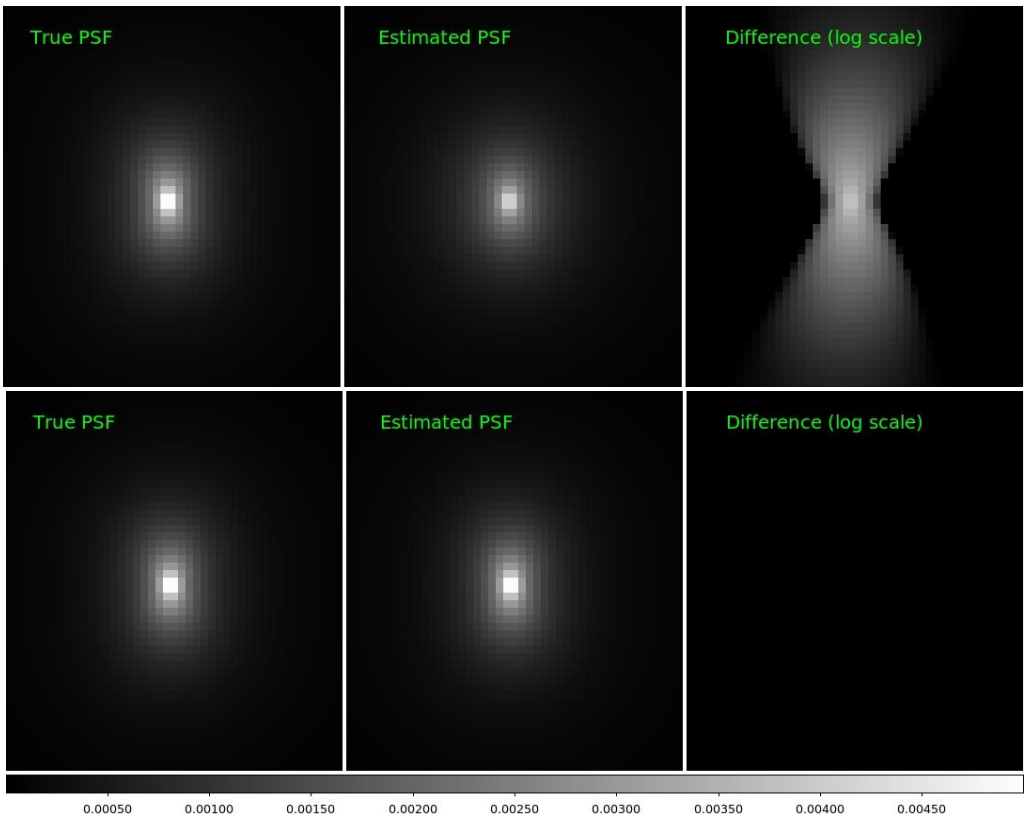

Fig. 8. Top row: PSF estimation with the marginal criterion. Bottom row: PSF estimation with the marginal criterion and positivity on the object. Leftmost panels: ground-truth PSFs. Middle panels: estimated PSFs. Rightmost panels: difference between the real PSF and the estimated one (log scale). Object mean flux equals 10^3 photons per pixel.

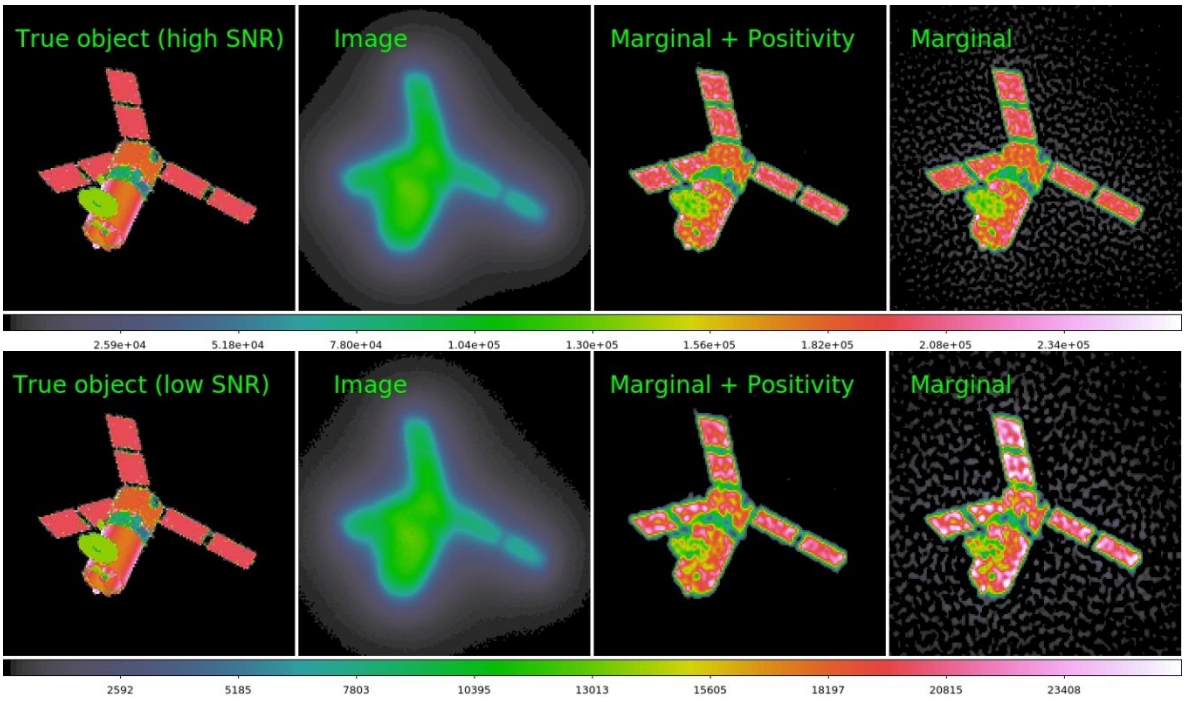

Fig. 9. Top row: results at high SNR, object mean flux equal to 10^4 photons/pixel. Bottom row: results at low SNR, object mean flux equal to 10^3 photons/pixel. First column: ground truth object. Second column: simulated image after convolution with AO long-exposure PSF in Figure 7 (top row, third column). Photon noise plus read out noise ($1e^-$ RMS) were consecutively added. Third column: results from the marginal criterion with positivity on the object. An explicit object is obtained at each iteration; these results show the restored object at the last iteration. Fourth column: results from the marginal criterion with no positivity on the object. An implicit object is computed using the Wiener solution for a given PSF, hence, the final object is obtained using the final PSF and the Wiener filter.

5. Conclusions

In the second year of the project we have introduced a novel way of extracting a PSF from sequence of images of arbitrary objects. The method is applicable to astronomical imaging with AO and to imaging with small apertures and/or long wavelengths. Especially interesting will be the application of the new approach to estimation of spatially-varying PSF in single-conjugate AO imaging. Based on experience with real data from Starfire Optical Range we posit that the method will work with less than 100 images. There is also nothing preventing the use of the method with long exposures: the only thing that will change will be then the number of random phasors N which will correspondingly increase. Practical issue might arise in that both contrast and skewness diminish towards zero when N increases (see Equation (6)). This might lead to degeneracy of the solution and theoretical work is already underway to find more accurate models for speckle statistics [15]. This and other issues, especially pertaining to anisoplanatic deconvolution based on singular value decomposition of the reconstructed local PSFs, will be explored in Year 3 of the project.

We also have extended the marginal blind deconvolution from the context of retinal imaging towards the identification of satellites observed with single-conjugate AO systems. The marginal criterion has been modified to include constraints on the object, such as positivity, in order to make the PSF estimation more robust in the presence of noise [16]. This approach can be extended to the anisoplanatic case by its application to different positions in the FOV as an essential building block of a global, shift-variant image

restoration method. Additionally, we plan to create a large dictionary of PSFs, describing different atmospheric conditions, from which marginal blind deconvolution will extract the correct linear combination of PSF coefficients at each position. In order to help the convergence of the algorithm different constraints over the PSF can be applied, such as sparsity on the coefficients through an l1 regularization in order to force the real PSF to a be a linear combination of only a few of the PSFs within the dictionary, and/or constraining the shape and orientation of the PSF to correspond with its position in the FOV.

Main research thrust in Year 3 will be devoted to development of a novel kind of simulation tool which will allow for rapid generation of anisoplanatic image sequences for three scenarios: uncompensated, horizontal-path imaging with very small isoplanatic angles, single-conjugate AO-compensated vertical imaging, and air-to-ground, "looking-down", slant-path scenario. Some work on the theory behind such a simulation has been carried out in Year 2 of the project [17].

The methods of PSF estimation and anisoplanatic deconvolution developed in the course of the project until now would then be tested on these simulated sequences.

6. References

1. Baena Gallé, R., Gladysz, S., Mateos, J., "Anisoplanatic Imaging through Turbulence Using Principal Component Analysis," Proceedings of the AMOS Technical Conference, Maui, 15-18 September (2015).

2. Gladysz, S., Baena Gallé, R., Johnson, R., Kann, L., "Image reconstruction of extended objects: demonstration with the Starfire Optical Range 3.5m telescope," in Optics in Atmospheric Propagation and Adaptive Systems XV, Karin Stein; John Gonglewski, Editors, Proceedings of SPIE Vol. 8535, 85350M, (2012).

3. Gladysz, S., "Adaptive optics point spread function reconstruction directly from target data," in Adaptive Optics: Analysis, Methods & Systems, 25 - 28 July 2016, The Optical Society, (2016).

4. Véran, J.-P., Rigaut, F., Maître, H., Rouan, D., "Estimation of the adaptive optics long-exposure point-spread function using control loop data," JOSA A 14, (1997).

5. Jolissaint, L., Carfantan, H., Anterrieu, E., "Exploring the impact of PSF reconstruction errors on the reduction of astronomical adaptive optics based data," Proc.SPIE, 7015, 159 (2008).

6. Jolissaint, L., Christou, J., Wizinowich, P., Tolstoy, E., "Adaptive optics point spread function reconstruction: lessons learned from on-sky experiment on Altair/Gemini and pathway for future systems", Proc. SPIE 7736, Adaptive Optics Systems II, 77361F (2010).

7. Uozumi, J., Asakura, T., "The first-order statistics of partially developed non-Gaussian speckle patterns," J. Opt. 12, 177-186 (1981).

8. Yaitskova, N., Esselborn, M., Gladysz, S., "Statistical moments of the Strehl ratio," Proc. SPIE 8447, 84475Y (2012).

9. Blanco, L. and Mugnier, L., "Marginal blind deconvolution of adaptive optics retinal images," Optics Express, 19, 23227-23239, 2011.

10. Conan, J.M., Mugnier, L.M., Fusco, T., Michau, V. and Rousset, G. "Myopic deconvolution of adaptive optics images by use of object and point-spread function power spectra". Applied Optics, 37, 4614-4622, 1988.

11. Baena Gallé, R., Núñez, J., Gladysz, S., "Extended Object Reconstruction in Adaptive-optics Imaging: The Multiresolution Approach," Astronomy & Astrophysics, 555, A69, (2013).

12. Jolissaint, L., Véran, J.-P. and Conan, R., Analytical modeling of adaptive optics: foundations of the phase spatial power spectrum approach, *JOSA A*, Vol. 23, 382-394, 2006.

13. Johnson, R., Montera, D., Schneeberger, T. and Spinhirne, J., "A New Sodium Guidestar Adaptive Optics System for the Starfire Optical Range 3.5m Telescope", in Frontiers in Optics 2009/Laser Science XXV, OSA Optics & Photonics Technical Digest, OSA Technical Digest (CD), 2009.

14. http://www.eso.org/sci/facilities/eelt/science/drm/tech_data/ao/

15. Yaitskova, N., Gladysz, S., "Statistics of adaptive optics speckles: from probability cloud to probability density function," in Adaptive Optics: Analysis, Methods & Systems, 25 - 28 July 2016, The Optical Society, (2016).

16. Baena Gallé, R., Mugnier, L., Gladysz, S. "Marginal blind deconvolution of AO corrected images of satellites" in Adaptive Optics: Analysis, Methods & Systems, 25 - 28 July 2016, The Optical Society, (2016).

17. Hardie, R. C., Power, J. D., LeMaster, D., Droege, D. R., Gladysz, S. and Basu, S., "Simulation of Anisoplanatic Imaging Through Optical Turbulence Using Numerical Wave Propagation," to be submitted to Optical Engineering

7. List of Symbols, Abbreviations, and Acronyms

AO – adaptive optics

AMOS – Air Force Maui Optical and Supercomputing

AWMLE – Adaptive Wavelet Maximum Likelihood Estimator

FOV – field of view

GS – guide star

MTF – modulation transfer function

ORS – Operationally Responsive Space-1 satellite

OTF – optical transfer function

PSF – point-spread function

R-L – Richardson-Lucy algorithm

RMS – root mean square (standard deviation)

SNR – signal-to-noise ratio

TV – total variation constraint